JGR Atmospheres

RESEARCH ARTICLE
10.1029/2019JD032093

Impacts of Tiled Land Cover Characterization on Global Meteorological Predictions Using the MPAS-A

Patrick C. Campbell[1,2,3], **Jesse O. Bash**[4], **Jerold A. Herwehe**[4], **Robert C. Gilliam**[4], **and Dan Li**[5]

[1]National Academies/National Research Council (NRC) Fellowship Participant at National Exposure Research Laboratory, U.S. Environmental Protection Agency, Research Triangle Park, NC, USA, [2]Now at Center for Spatial Information Science and Systems/Cooperative Institute for Satellite Earth System Studies, George Mason University, Fairfax, VA, USA, [3]Office of Air and Radiation, Air Resources Laboratory, National Oceanic and Atmospheric Administration, College Park, MD, USA, [4]Center for Environmental Measurement and Modeling, U.S. Environmental Protection Agency, Research Triangle Park, NC, USA, [5]Department of Earth and Environment, Boston University, Boston, MA, USA

Abstract Parameterization of subgrid-scale variability of land cover characterization (LCC) is an active area of research and can improve model performance compared to the dominant (i.e., most abundant tile) approach. The "Noah" land surface model implementation in the global Model for Prediction Across Scales-Atmosphere (MPAS-A), however, only uses the dominant LCC approach that leads to oversimplification in regions of highly heterogeneous LCC (e.g., urban/suburban settings). Thus, in this work we implement a subgrid tiled approach as an option in MPAS-A, version 6.0, and assess the impacts of tiled LCC on meteorological predictions for two gradually refining meshes (92–25 and 46–12 km) focused on the conterminous United States for January and July 2016. Compared to the dominant approach, results show that using the tiled LCC leads to pronounced global changes in 2-m temperature (July global average change approximately −0.4 K), 2-m moisture, and 10-m wind speed for the 92–25 km mesh. The tiled LCC reduces mean biases in 2-m temperature (July U.S. average bias reduction approximately factor of 4) and specific humidity in the central and western United States for the 92–25 km mesh and improves the agreement of vertical profiles (e.g., temperature, humidity, and wind speed) with observed radiosondes; however, there is increased bias and error for incoming solar radiation at the surface. The inclusion of subgrid LCC has implications for reducing systematic temperature biases found in numerical weather prediction models, particularly those that employ a dominant LCC approach.

Key Points:
- The use of tiled land cover characterization (LCC) has significant impacts on global meteorological predictions in MPAS-A
- Tiled LCC reduces bias and error for near-surface temperature, moisture, and wind speed over the United States
- The tiled LCC approach is important and can help mitigate systematic temperature biases in weather and climate models

Supporting Information:
- Supporting Information S1

Correspondence to:
P. C. Campbell,
patrick.c.campbell@noaa.gov

Citation:
Campbell, P. C., Bash, J. O., Herwehe, J. A., Gilliam, R. C., & Li, D. (2020). Impacts of tiled land cover characterization on Global Meteorological Predictions Using the MPAS-A. *Journal of Geophysical Research: Atmospheres*, *125*, e2019JD032093. https://doi.org/10.1029/2019JD032093

Received 6 DEC 2019
Accepted 19 JUN 2020
Accepted article online 23 JUN 2020

1. Introduction

The land cover characterization (LCC), that is, the physical characteristics of Earth's land surface (vegetated, wetlands, water, ice, or urban/impervious), is inherently heterogeneous and is rapidly changing due to recent and projected future fluctuations in the LCC for both developed and developing countries. Changes in LCC due to human activities (e.g., deforestation, industrialization, agriculture, and urban sprawl) produce physical changes in land surface albedo, latent (LH) and sensible heat (SH) fluxes, and atmospheric aerosol and greenhouse gas concentrations. Consequently, there is high confidence that changes in LCC and the feedbacks to surface properties, fluxes, and atmospheric composition account for as much as half of the human-caused global radiative forcing from 1850 to the present day (Hibbard et al., 2017).

Numerical weather predictions (NWPs) and climate models are used to predict the near- and long-term weather and climate changes, respectively, and are tightly bound to the land surface model (LSM) component that represents the lower physical boundary. The LSM component also controls the representation of LCC variability, is the memory of climatic changes, and apportions the physical responses in surface LH and SH fluxes. NWP models, however, consistently simulate warmer surface temperatures compared to ground observations, where most of the systematic 2-m temperature biases appear by Day 5 predictions, and the largest warm bias is found in the Central United States (Ma et al., 2014). A joint model-observation intercomparison project, the Clouds Above the United States and Errors at the Surface (CAUSES), evaluated the role of clouds, radiation, and precipitation processes in contribution to the surface temperature biases in the Central United States (Morcrette et al., 2018). One of the important findings from

the CAUSES project was that the large warm bias in NWP models is attributed to the simulation of deep convective clouds and the evaporative fraction (EF = LH/[LH + SH]) at the surface (Steiner, 2018; and references contained within). As the EF is strongly tied to the LCC, we extend this connection to assert that there also exists a relationship between the accuracy of the NWP models' representation of the LCC and subgrid scale variability in its coupled LSM, and the predictive accuracy of EF and associated feedbacks with surface temperature and moisture, clouds, and precipitation.

The need for subgrid-scale LCC variability in LSMs has been known for some time and has been an active area of research over the past three decades (Giorgi & Avissar, 1997). Avissar and Pielke (1989) first proposed a subgrid LCC parameterization that used a number of patches (or tiles), that is, the "tiled" approach, and showed that it resulted in strong contrasts in total surface energy fluxes. In the tiled approach, the corresponding surface fluxes, energy, and water balances in the LSM are calculated for each explicit LCC with unique vegetation attributes in the model grid cell and then are spatially averaged to produce the surface fluxes for each cell. Other subgrid LCC approaches are also found in multi-mode, offline/coupled land-ocean surface platforms, such as the "SURFEX" model (Masson et al., 2013). Other subgrid LCC methods include the "composite" approach, which is similar to the dominant approach, but the surface properties are either linearly or nonlinearly aggregated based on the properties of all the tiles within the grid cell (Koster & Suarez, 1992; Verseghy et al., 1993). The statistical-dynamical approach assumes that the land surface parameters that are critical for calculating surface fluxes follow certain probability density functions (PDFs) (Avissar, 1991; Entekhabi & Eagleson, 1989; Famiglietti & Wood, 1991). The multivariate mosaic subgrid approach (i.e., "k-means clustering") method is used to take an arbitrary number of input descriptors and objectively determine areas of similarity within a grid cell. This is in contrast to a "univariate approach" that only uses one spatially varying parameter to aggregate a catchment into a relatively few classes (Newman et al., 2014). The k-means clustering method may in fact be well suited to represent subgrid spatial complexity in LSM applications on the global to regional scales. Other global- to regional-scale LSMs have incorporated subgrid LCC, such as the Community Land Model (CLM) that has a nested subgrid hierarchy in which grid cells are composed of multiple land units (vegetated, lake, urban, glacier, and crop), snow/soil columns, and plant functional types (PFTs). A true tiled scheme called "newsnow" is also an option in the European High Resolution Limited Area Model (HIRLAM), and it includes seven individual subgrid tiles that are treated with unique values of vegetation, roughness length, and albedo (Gollvik & Samuelsson, 2011; Samuelsson et al., 2006).

On the contrary, the application of a "dominant" approach to LCC in LSMs, where each grid cell is assumed to be entirely composed of the most abundant LCC type, is a known oversimplification of the real-world LCC variability (realistically on the order of meters), even at relatively "high-resolution" mesoscale simulations (<10 km) (Ament & Simmer, 2006). This becomes a greater issue for global-scale NWP or climate models, which are typically run at coarser horizontal resolutions (e.g., ~100 km or greater). Of course, in practice, there must exist a balance between representing the myriad of processes that relatively coarse models cannot resolve, especially global climate models, and the available computational capacity and resources for the respective application of the model.

The unified National Center for Atmospheric Research (NCAR), Oregon State University, the U.S. Air Force, and National Centers for Environmental Prediction's (NCEP's) Office of Hydrology ("Noah") LSM (Chen & Dudhia, 2001; Chen et al., 1996, 1997, 2007; Ek et al., 2003; Li et al., 2013; Mitchell et al., 2004; Niu et al., 2011; Pan & Mahrt, 1987; Yin et al., 2015) has been widely developed, applied, and evaluated in its parent atmospheric grid model, the Weather Research and Forecasting (WRF) model (Powers et al., 2017; Skamarock & Klemp, 2008). The Li et al. (2013) method of explicit tiling (referred to as the "mosaic" method) in WRF/Noah is intriguing as it maintains tile-specific surface energy flux calculations that are then weighted averages for the entire grid cell used in conservation checks. Furthermore, Li et al. demonstrated that the tiled LCC method demonstrates stark differences, better model performance, and less sensitivity to spatial grid resolution for surface energy fluxes, land surface temperature, near-surface states, boundary layer growth, and rainfall distribution compared against the dominant approach in Noah. However, the applications of tiled LCC in global LSMs are limited to simulated energy and carbon balances at select boreal, temperate, and tropical locations across the world (Li & Arora, 2012) and do not truly investigate the global, coupled atmospheric feedbacks as a result of the tiling (Melton & Arora, 2014). Furthermore, studies that do investigate such atmospheric feedbacks to subgrid LCC are specific to regional-scale applications (Li &

Arora, 2012; Li et al., 2013, 2017; Mallard & Spero, 2018). We note that the above referenced studies show that certain surface parameters and energy fluxes may be sensitive to using a tiled LCC compared to a dominant or composite approach. Thus, there is a need to implement and carefully test the impacts of tiled LCC on the global scale to assess the impacts of more realistic LCC on surface energy fluxes and the feedbacks to the cloud and radiative model predictions. The effects of tiled LCC have implications for both the scientific and operational weather forecasting communities, especially in areas of highly contrasting LCC types (Manrique-Suñén et al., 2013).

The atmospheric component of the Model for Prediction Across Scales-Atmosphere (MPAS-A) uses an unstructured centroidal Voronoi, nominally hexagonal mesh (grid, or tessellation) and C-grid staggering of the state variables as the basis for the horizontal discretization in the dynamical solver (Skamarock et al., 2012, and references contained within). The MPAS-A is ideal for this work as it is a parent, global atmospheric model to the Noah LSM, and the unstructured variable resolution meshes can be generated having smoothly varying mesh transitions. The Noah implementation in MPAS-A (hereafter referred to as MPAS/Noah), however, only uses the dominant LCC approach. This results in an oversimplification in regions of highly heterogeneous LCC (e.g., urban/suburban settings), which is also impacted by the gradually refining meshes in MPAS for global to mesoscale applications. Thus, in this work we implement the tiled LCC approach as an option in MPAS/Noah, version 6.0, and assess the global-to-mesoscale impacts of tiled LCC in MPAS/Noah on meteorological predictions for two gradually refining meshes (92–25 and 46–12 km) focused on the conterminous United States (CONUS) for January and July 2016. The year 2016 was chosen as relatively fine scale initial conditions are available for that year (see section 2.2), and the January/July months represent climatological cool/warm seasons for both the Northern and Southern Hemispheres.

2. Methods

2.1. A Tiled Approach to LCC in MPAS-A

In this work we implement a tiled LCC to MPAS/Noah, which is analogous to the tiled (i.e., "mosaic") approach found in the WRF model described by Li et al. (2013) (hereafter referred to as the "L13-tiled," or simply the "tiled" approach). Generally applying the L13 approach here, a certain user-defined number (N) of tiles, each representing a land cover category, is considered within a mesh cell. The atmospheric properties and soil properties are assumed to be homogenous over the mesh cell when surface fluxes and surface state variables are calculated for each tile, and all prognostic variables are maintained for each tile, some of which are aggregated to yield the mesh cell average variables (Li et al., 2013). In the L13-tiled approach the mesh cell average variables are weighted by the normalized area fraction accounting for the areas of each tile, where the tile with the largest normalized area fraction has a rank of 1. The smaller normalized area fractions for each land cover category are subsequently given lower rankings, and the total N tiles are assumed constant for all mesh cells. This is in contrast to the dominant LCC approach, which only considers the most dominant tile (i.e., tile rank = 1), and does not consider fractional impacts of subgrid, tiled heterogeneity in LCC (Figure 1). The reader is referred to Li et al. (2013) and the references contained within for further details regarding the L13-tiled approach.

2.2. Model Configuration and Simulation Design

Here we apply two MPAS-A version 6.0 global meshes that seamlessly refine from a relatively coarse to fine, 92–25 and 46–12 km, horizontal grid spacing over the CONUS. The global domain and subset of the CONUS are shown for the 92–25 km mesh in Figure 2, which also include the corresponding average vegetation fractions for January and July 2016.

The meteorological initial conditions are based on NCEP operational Global Forecast System analysis and forecast grids on a 0.25° × 0.25° global latitude longitude grid (https://rda.ucar.edu/datasets/ds083.3/). A combined 40-category data set is used to represent the LCC, where the National Land Cover Database (NLCD) is used within the CONUS, and elsewhere the International Geosphere-Biosphere Programme (IGBP)-Modified Moderate Resolution Imaging Spectroradiometer (MODIS) satellite database. Independent tests of a similar WRF model configuration/domain over the United States also indicate that setting the number of tiles (N) = 8 results in about 97% of all model grid cells having 99% of their LCC categories represented (Campbell et al., 2019). To ensure all MPAS/Noah mesh cells have ≥99% of their LCC categories represented, here we employ a very conservative value of $N = 15$.

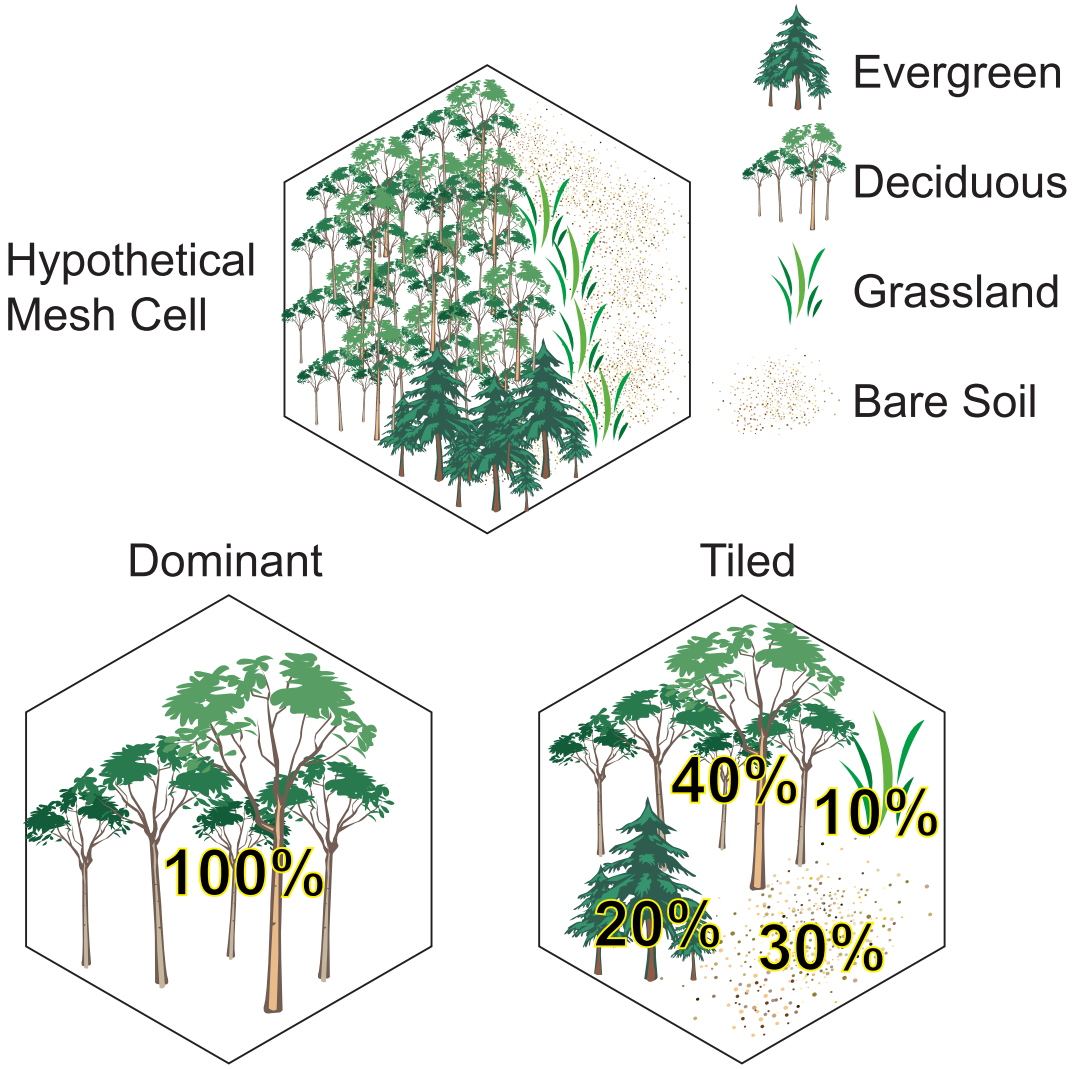

Figure 1. Illustration of a hypothetical "real-world" land cover in a hexagonal mesh cell in MPAS-A, and the corresponding dominant versus L13-tiled approach to LCC used in the MPAS/Noah LSM.

The simulation design consists of 1-month simulations using dominant and tiled LCC for January and July 2016, at both 92–25 and 46–12 km variable mesh grid spacing (total of eight simulations). Each simulation applies a continuous 10-day spin-up (not used in analysis) and a collection of 5-day reinitializations (Table 2), with no overlaps, which both reduces the error ingested from the initial conditions and helps avoid model divergence typical of longer simulation periods (e.g., multiple weeks or months).

Table 1
MPAS-A v6.0 Model Configuration

Model mesh/process	Configuration
Mesh resolutions with seamless refinement	92–25 km and 46–12 km
Time steps	100 s (92–25 km); 40 s (46–12 km)
Land surface model	Dominant and *L13-tiled Noah* ($N = 15$ tiles per cell)
LCC data	Combined 40-category NLCD (conterminous United States) and IGBP-MODIS (global)
Surface layer	Monin-Obukhov (MO)
Planetary boundary layer	Yonsei University (YSU)
Grid microphysics/subgrid convection	WRF Single Moment 6-class (WSM6)/Kain-Fritsch (KF)
Radiation	Rapid Radiative Transfer Model for GCMs (RRTMG)

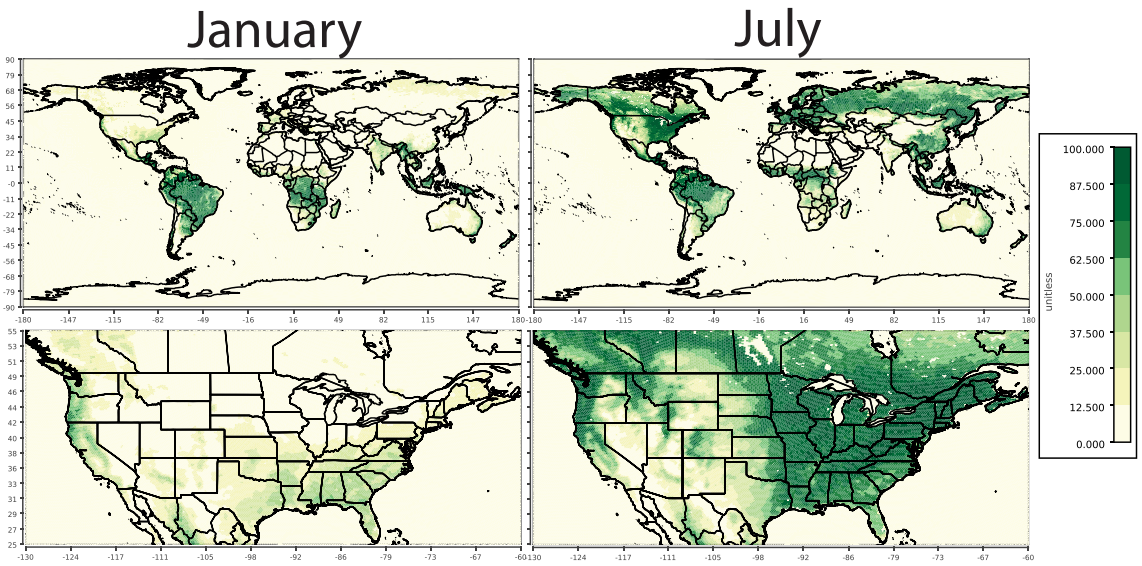

Figure 2. Global 92–25 km and seamlessly refined 25 km mesh over CONUS. The average vegetation fraction at 92–25 km is also shown for January and July 2016. Here we employ the default MPAS-A v6.0 default physics suite (based on the Advanced Research WRF model), except for the new implementation of the L13-tiled approach as an option to dominant LCC (default) in MPAS/Noah (Table 1). The physics options used here are a very common configuration in WRF and thus are well documented on the WRF User's Page and references contained within (http://www2.mmm.ucar.edu/wrf/users/).

The simulation design in Table 2 allows for the analysis of the impacts of L13-tiled compared to dominant LCC during both a winter and summer month, while also providing insight into the impact of the L13-tiled approach on reduction of the sensitivity of the MPAS/Noah model to different mesh resolutions.

2.3. Observations and Evaluation Protocol

Observations from both surface and upper-air platforms are used for the evaluation of MPAS-A dominant versus the tiled method and the sensitivity to the refining mesh resolution. The near-surface observations of 2-m temperature (T2), 2-m specific humidity (Q2), and 10-m wind speed (WSPD10) are based on the Surface Weather Observations and Reports for Aviation Routine Weather Reports (METAR) which are collected by NCEP's Meteorological Assimilation Data Ingest System (MADIS) (https://madis.ncep.noaa.gov/madis_metar.shtml). The shortwave radiation at the ground (SWDOWN) observations are obtained from the World Radiation Monitoring Center's (WRMC's) Baseline Solar Radiation Network (BSRN) (https://bsrn.awi.de/; Driemel et al., 2018). Vertical profile observations of temperature, relative humidity, and wind speed are obtained from the National Oceanic and Atmospheric Administration (NOAA), Earth System Research Laboratory's (ESRL's) Radiosonde Database (RAOB) (https://ruc.noaa.gov/raobs/).

Typical meteorological statistical metrics are used to evaluate the performance of MPAS-A dominant versus the tiled approach, which include the mean bias (MB), root mean square error (RMSE), Pearson's correlation coefficient (R), and index of agreement (IOA). Such statistical metrics have been well defined in the available literature (e.g., Table 3 in Emery et al., 2017).

Table 2
MPAS-A v6.0 Model Simulation Design

Run	MPAS/Noah LCC	Period	Mesh resolution (km)
#1	Dominant	January 2016	92–25
#2	Dominant	July 2016	92–25
#3	L13-tiled	January 2016	92–25
#4	L13-tiled	July 2016	92–25
#5	Dominant	January 2016	46–12
#6	Dominant	July 2016	46–12
#7	L13-tiled	January 2016	46–12
#8	L13-tiled	July 2016	46–12

3. Results

3.1. Impacts of the Tiled Approach for the MPAS-A 92–25 km Mesh

Globally, the tiled method's top ranked tiles (i.e., ranking of LCC by dominance) show a high heterogeneity in LCC categories and associated fractions compared to the dominant category (Figures 3a–3f). In the western United States, the tiled method allows for forest fractions in cells dominated by grasses/shrubs, while in the eastern United States, there are urban and grass/shrub fractions in cells dominated by forest (Figures 3g–3l). Ultimately, the amount of tiled

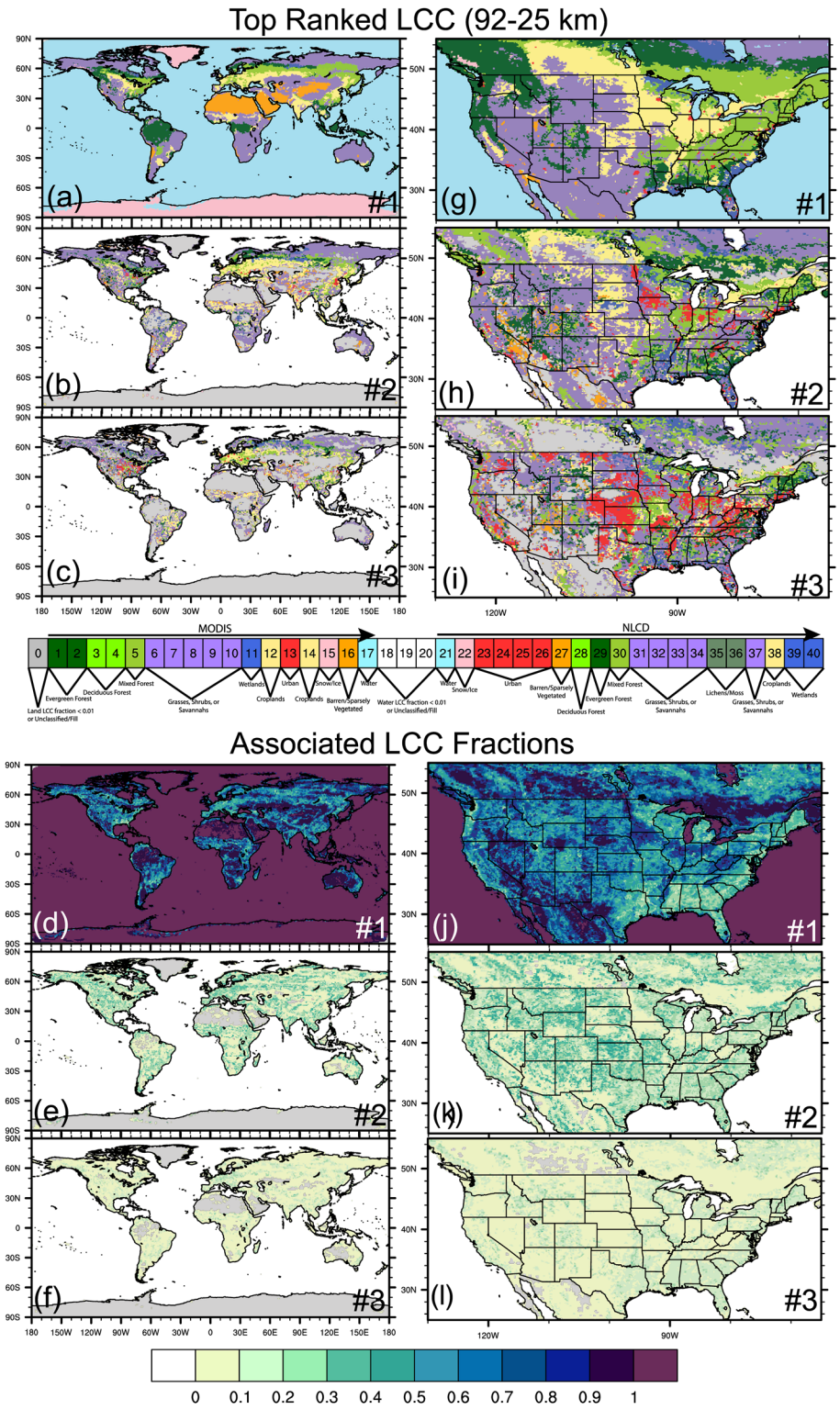

Figure 3. Spatial plots of the top three ranked (#1 = dominant LCC, #2, and #3) tiled LCC categories and their associated fractions for the combined 40-category NLCD (CONUS) and (IGBP)-Modified MODIS satellite database (elsewhere global). The IGPB-MODIS (1–17) and NLCD (21–40) LCC categories are (combined for simplification) forests: 1–5 and 28–30; grasses, shrubs, or savannahs: 6–10 and 31–34 and 37; lichens/moss: 35–36; wetlands: 11 and 39–40; croplands: 12, 14, and 38; urban/developed: 13 and 23–26; snow and ice: 15 and 22; barren/sparsely vegetated: 16 and 27; water: 17 and 21; and regions of LCC fraction <0.01 or unclassified: 0 (shaded gray for land) and 18–20 (shaded pure white for water). Areas with zero associated LCC fractions are also shaded in gray for land and pure white for water.

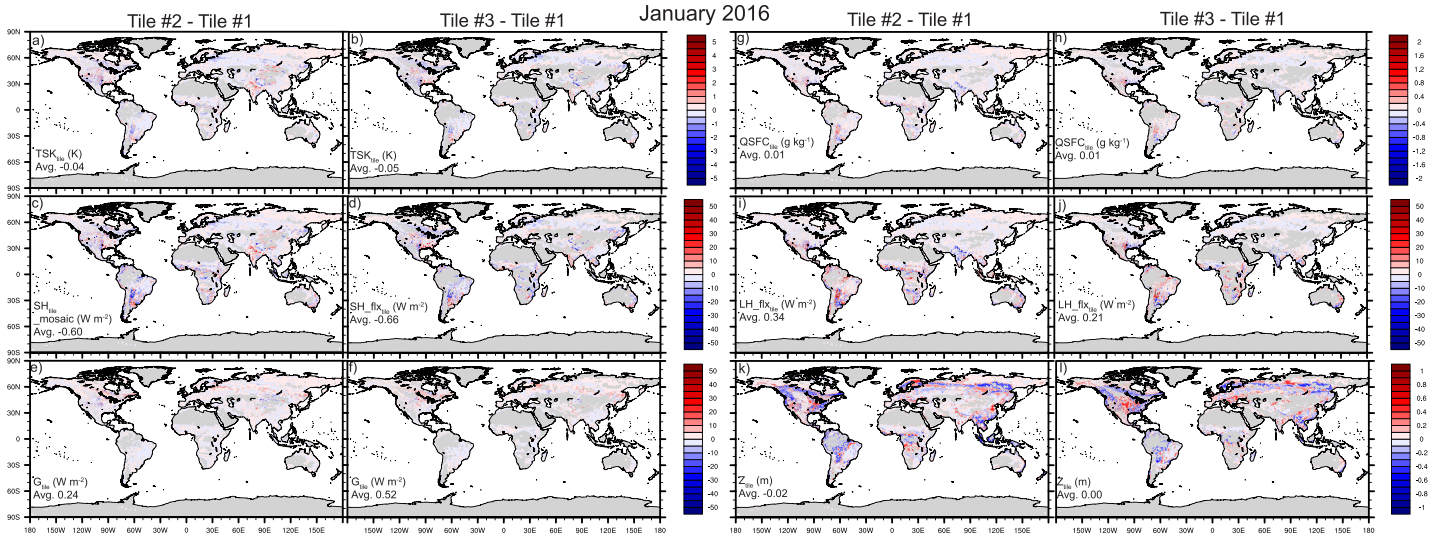

Figure 4. January 2016 average differences in the top ranked tiled LCC categories (#2-#1 and #3-#1) for (a, b) TSK_{tile}, (c, d) SH_{tile}, (e, f) G_{tile}, (g, h) $QSFC_{tile}$, (i, j) LH_{tile}, and (k, l) Z_{tile} on the 92–25 km resolution mesh. Areas shown in gray for land and white for water have zero change for each tiled variable and are not significant (see Figure 3 for LCC ranking and fraction).

LCC heterogeneity depends on the combination of the specific input LCC data set and model cell resolution, which in this case varies from the global (IGBP-MODIS and 92 km) to the U.S. scale (NLCD and 25 km).

Including additional LCC categories in the tiled method results in global differences for the top three ranked tiled (i.e., tile #2-#1 and #3-#1) surface/skin temperature (TSK_{tile}), surface specific humidity ($QSFC_{tile}$), sensible heat flux (SH_flx_{tile}), latent heat flux (LH_flx_{tile}), ground heat flux (G_{tile}), and aerodynamic roughness length (Z_{tile}) in January (Figure 4) and July 2016 (Figure 5) for the 92–25 km mesh (supporting information Figure S1 also shows the albedo, ALB_{tile}, and emissivity, $EMIS_{tile}$, differences). Clearly, the regions of appreciable LCC fractions for tile rankings #2 and #3 (Figure 3) spatially agree well with the areas of largest changes in surface variables and fluxes, where the magnitude of TSK change is generally larger in July (e.g., Figure 5a; global avg. $\Delta TSK_{tile\#2\text{-}\#1} = -0.13$ K) compared to January (e.g., Figure 4a; global avg. $\Delta TSK_{tile\#2\text{-}\#1} = -0.04$ K), especially at the refined mesh scale (~25 km) in the CONUS region that uses the NLCD.

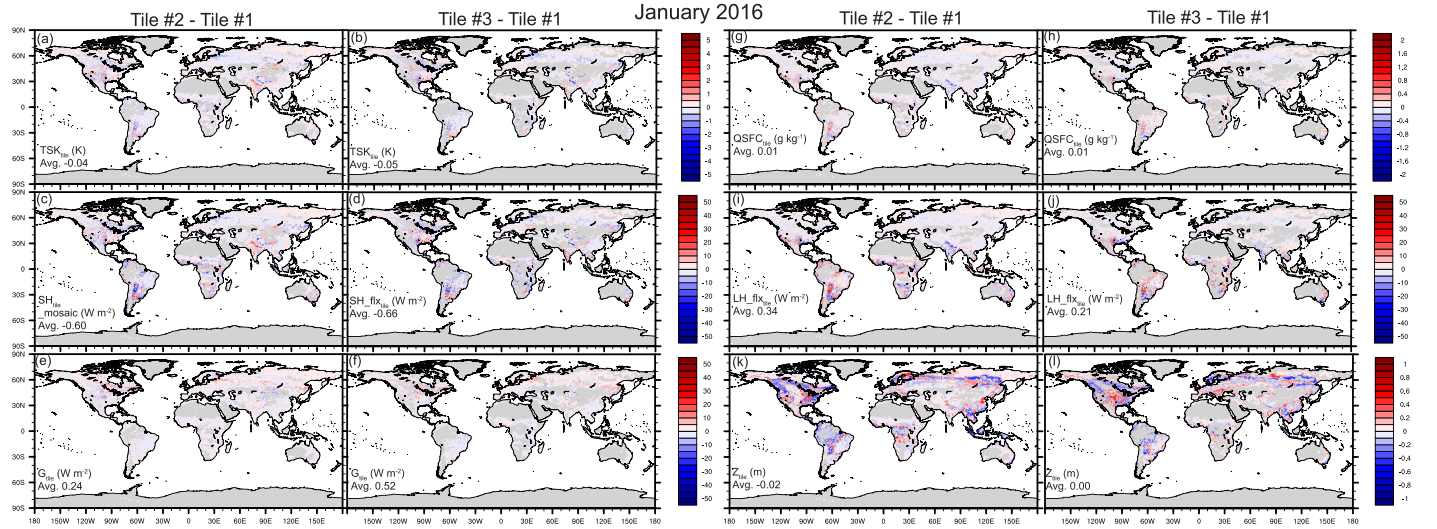

Figure 5. Same as in Figure 4, but for July 2016.

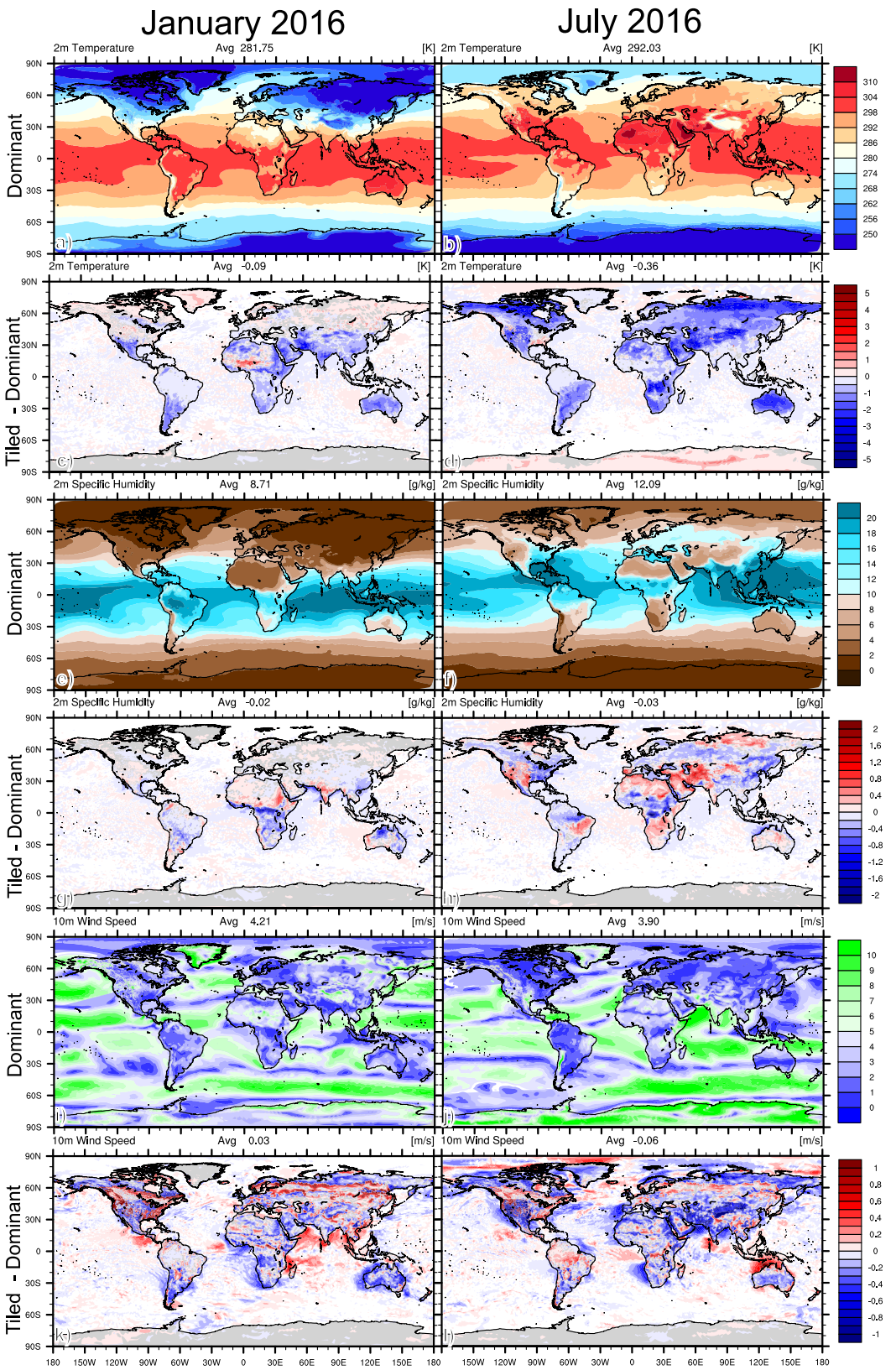

Figure 6. Average January (left) and July 2016 (right) dominant and difference plots (tiled-dominant) for the diagnostic variables (a–d) T2, (e–h) Q2, and (i–l) WSPD10 on the 92–25 km resolution mesh. Areas shaded as gray for land and pure white for water represent a *p*-value >0.05 and are statistically insignificant differences (tiled-dominant).

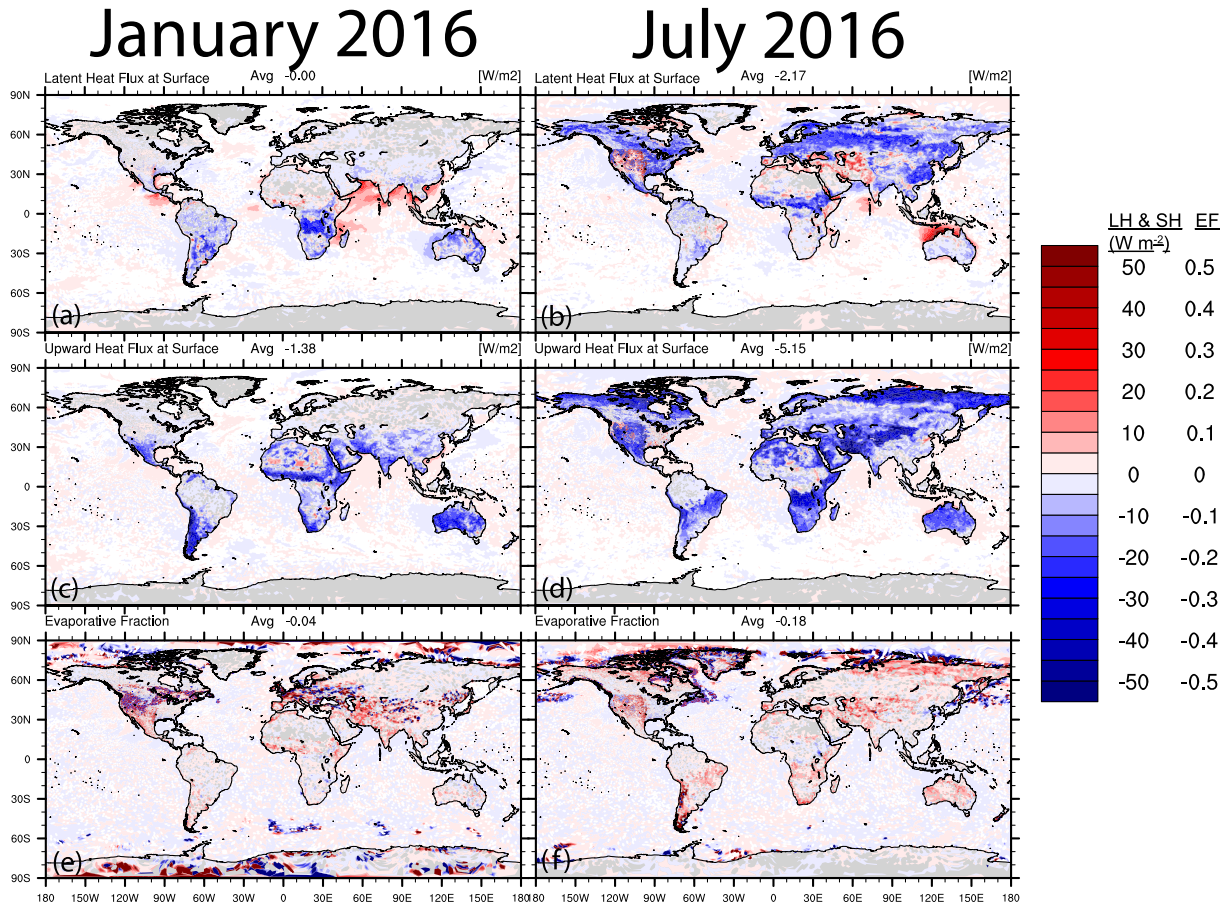

Figure 7. Average January (left) and July 2016 (right) difference plots (tiled-dominant) for (a, b) LH_flx, (c, d) SH_flx, and (e, f) evaporative fraction (EF) on the 92–25 km mesh. Areas shaded in gray for land and pure white for water represent a *p*-value >0.05 and are statistically insignificant differences (tiled-dominant).

On average, comparing the #2 and #3 ranked tiles to the dominant (#1 rank) leads to decreased global TSK_{tile} and SH_flx_{tile} and slightly increased G (more heat flux into the ground) in both January and July (Figures 4a–4f and 5a–5f). There are exceptions, however, where the #2 and #3 ranked LCC tiles demonstrate increased TSK_{tile}, SH_flx_{tile}, and G_{tile}, especially in the eastern CONUS for tiles #2-1 and #3-1 in July. These increases are due to the effects that urban and crop/grasslands in the #2 and #3 ranked tiles have on the surface energy balance compared to the dominant deciduous and evergreen forest in mesh cells found in this region (Figure 3). In the western United States in July, the #2 and #3 ranked tiles have appreciable fractions of forests compared to the dominant grasses, shrubs, or savannahs in this region that leads to a strong cooling effect with widespread decreases in TSK_{tile}, SH_flx_{tile}, and G_{tile}.

The tiled method also impacts the aerodynamic roughness length (Z_{tile}), which have the same changes for January and July 2016 because Z_{tile} is solely a function of the tabulated LCC category in the Noah LSM. On average, there is a slight decrease in Z_{tile} globally; however, there are locally larger increases and decreases dependent on the level of contrast in roughness lengths for different categories. For example, there are relatively large decreases in Z_{tile} in the eastern United States due to smaller average roughness lengths for croplands (~0.1; #2 and #3 ranked tiles) compared to the dominant forests (~0.5). Changes in roughness lengths, Z_{tile}, will have impacts on the diagnosed average wind speeds above the surface, as discussed further below.

There are prominent changes in the average January and July 2016 difference plots (tiled-dominant) for MPAS-A diagnostic variables T2, Q2, and WSPD10 at the 92–25 km resolution mesh (Figure 6). In fact, mostly all of the differences are deemed statistically significant based on a calculated *p*-value test statistic that is ≤0.05 for each cell. The *p*-value (i.e., probability) is used to determine the likelihood of a false null

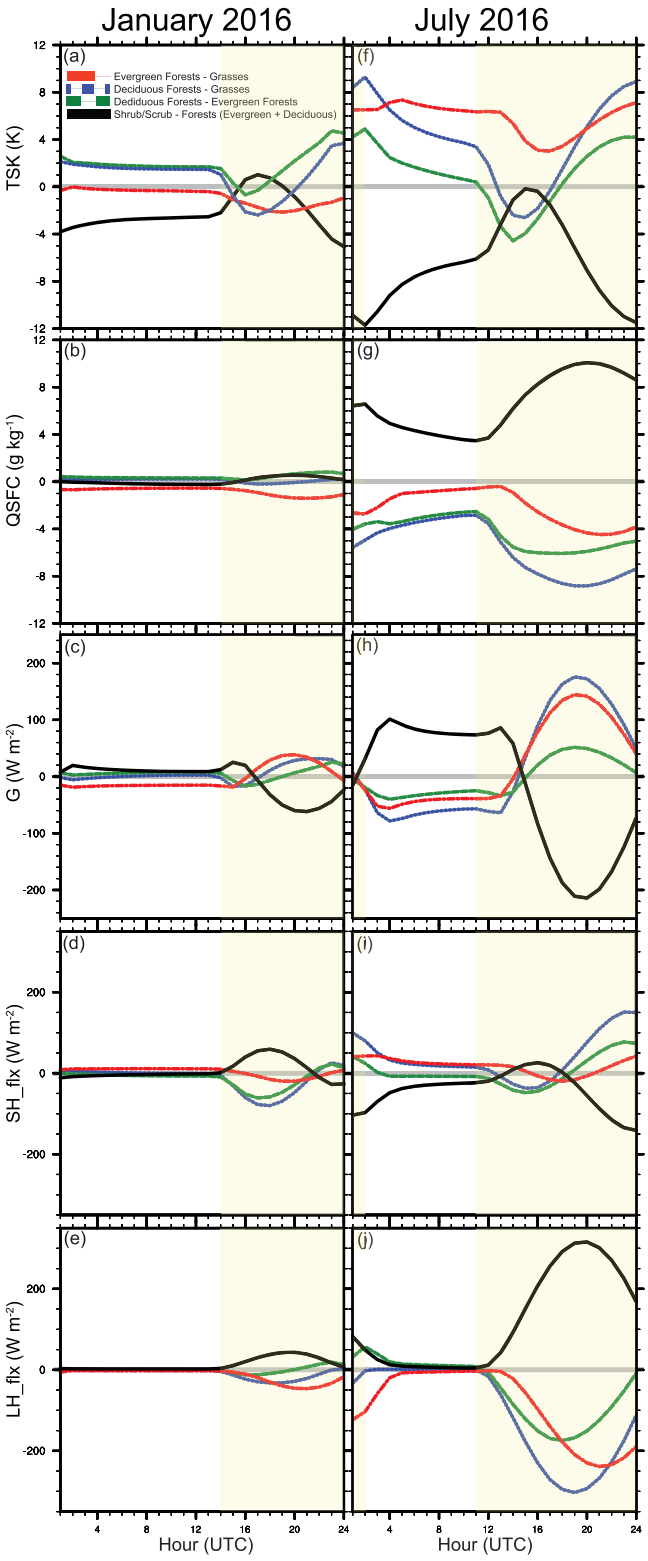

Figure 8. Diurnal analysis of the differences in dominant-second ranked tiles for TSK, QSFC, G, SH, and LH in (a–e) January and (f–j) July 2016. Analysis has been averaged over all CONUS grid cells. Approximate daytime hours for CONUS are shaded in light yellow/gray.

hypothesis, where the smaller the *p*-value, the higher the significant differences (tiled-dominant). There are only localized areas of statistically insignificant changes near the regions of smallest differences and are mostly found in January over the oceans and Antarctica (Figure 6; *p*-values >0.05 masked out as gray for land and white for water).

The globally widespread cooling in both January (approximately −0.1 K) and July 2016 (−0.4 K) in Figure 6 are due to global increases in LH_flx, widespread decreases in SH_flx, and consequently widespread increases in the EF (evaporative fraction; see section 1 for explanation), especially in July (Figure 7). These results suggest that using a tiled LCC may act to mitigate the systematic warm bias found in global NWP model applications that currently use a dominant LCC approach.

There is also a qualitative agreement for areas that are typical of higher (lower) temperatures (Figures 6a and 6b) with areas of decreased (increased) temperature due to tiled LCC (Figures 6c and 6d). The regions of lower (higher) humidity (Figures 6e and 6f) also agree with regions of increased (decreased) humidity (Figures 6g and 6h) due to tiling. The opposing directions of change in T2 and Q2, particularly for the United States in July (see dipoles of change in the west and east United States), further indicate that the impacts of the tiled method are a result of changes in the surface energy balance and a shift in the partitioning of the SH_flx and LH_flx, which is due to the incorporation of appreciable fractions of various LCCs in the mesh cells. There are spatially variable impacts on WSPD10 with both increases and decreases (Figures 6i and 6l), but the impact of the tiled LCC is largest in July and also leads to secondary (e.g., effects of modulated north-south temperature gradient) interactions in the northern high latitudes (approximately >60°N).

The impacts of the tiled method on EF also have feedbacks to the topmost soil temperature (TSLB) and moisture (SMOIS), as well as the planetary boundary layer height (PBLH) (Figure S2). In January, the TSLB increases in the high northern latitudes and decreases in the low northern latitudes and Southern Hemisphere. The increases (decreases) in TSLB qualitatively agree with decreases (increases) in SMOIS due to the effects of EF changes. In July, the effects are similar but exacerbated, where there are widespread decreases in TSLB and increases in SMOIS, respectively, which is most prominent in the Northern Hemisphere middle- to high-latitude regions, and may also be impacted by increases in the low cloud fraction (not shown). As expected, the increases (decreases) in PBLH are spatially well correlated with the regions of increases (decreases) in T2.

The spatial differences in tiled and diagnostic variables in January and July 2016 (Figures 4–6) are further elucidated when comparing the diurnal patterns of tiled G, LH, SH, QSFC, and TSK for the dominant and second ranked LCC category, most notably in July (Figure 8).

In much of the central and western United States, the widespread shrubs/grasses dominate the landscape (Figure 1), where including appreciable fractions of evergreen and deciduous forest in the tiled approach leads to a net increase in heat flux into the ground

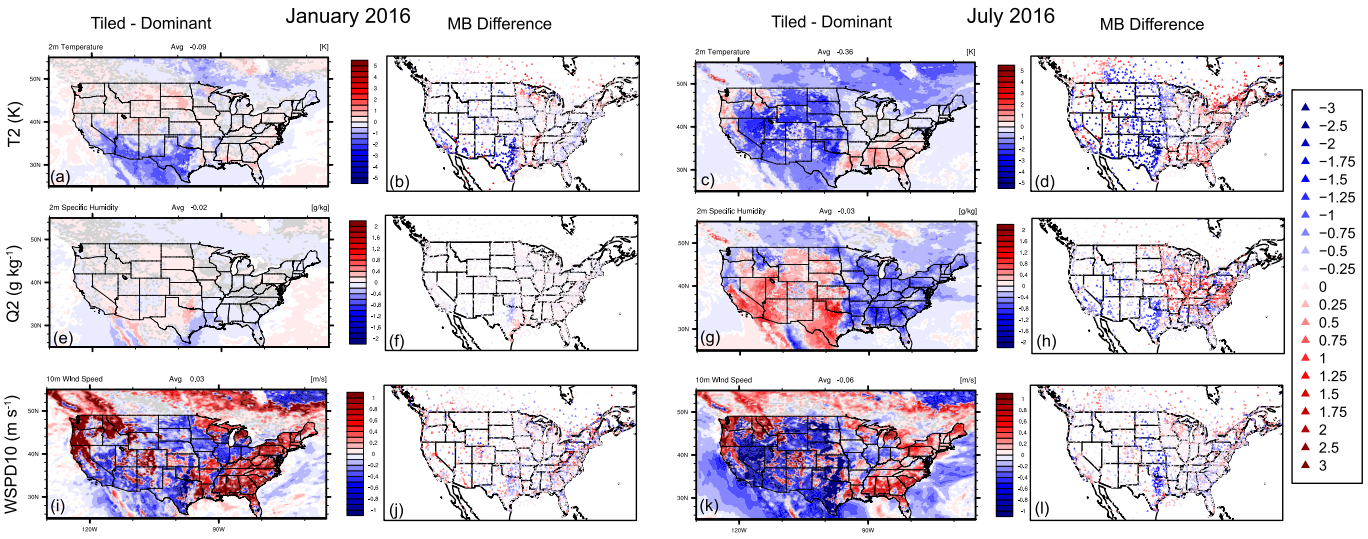

Figure 9. Average January (left) and July 2016 (right) absolute and MB difference (|tiled MB|-|dominant LCC MB|) compared against available MADIS-METAR stations for (a–d) T2, (e–h) Q2, and (i–l) WSPD10 on the 92–25 km resolution mesh. Areas shaded in gray for land and pure white for water represent a *p*-value >0.05 and are deemed statistically insignificant differences (tiled-dominant).

($\Delta G > 0$) at the expense of sensible heat flux ($\Delta SH < 0$), which results in cooler surface temperatures ($\Delta TSK < 0$) at night in July (black line; Figures 8f–8j). During the morning transition period, the ΔG, ΔSH, and change in latent heat flux (ΔLH) approach zero, and there is a minimum in ΔTSK due to the tiled effects. Later in the daytime hours in July, however, the presence of more evergreen and deciduous forest result in a net loss of ground heat flux ($\Delta G < 0$), which mostly enhances latent heat flux to the atmosphere ($\Delta LH > 0$), where energy partitioning also requires that $\Delta SH < 0$ and consequently cooler surface temperatures, $\Delta TSK < 0$. There is also a net increase in specific humidity ($\Delta QSFC > 0$) during both night and day in July due to the presence of more forest canopy and enhanced evapotranspiration (black line; Figures 8f–8j). The opposite is true when including tiled fractions of shrubs/grasses in either the dominant evergreen or deciduous forest regions, which are found mainly in the eastern United States,

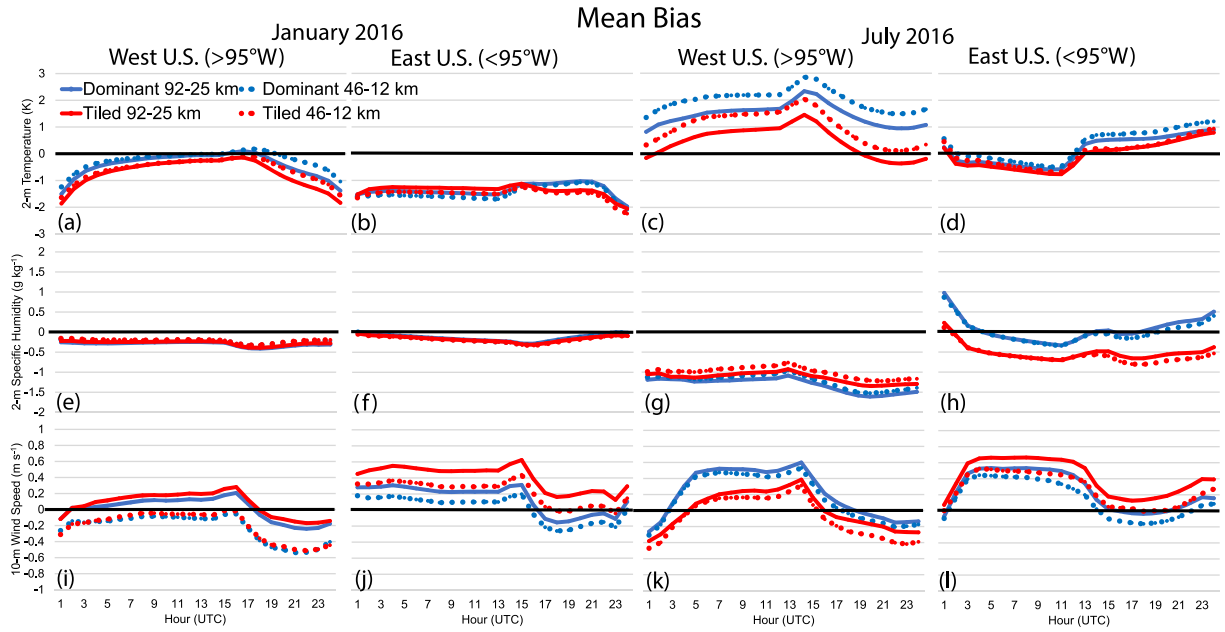

Figure 10. Diurnal MB comparisons for (a–d) T2, (e–h) Q2, and (i–l) WSPD10 against MADIS-METAR for 92–25 and 46–12 km over eastern and western CONUS.

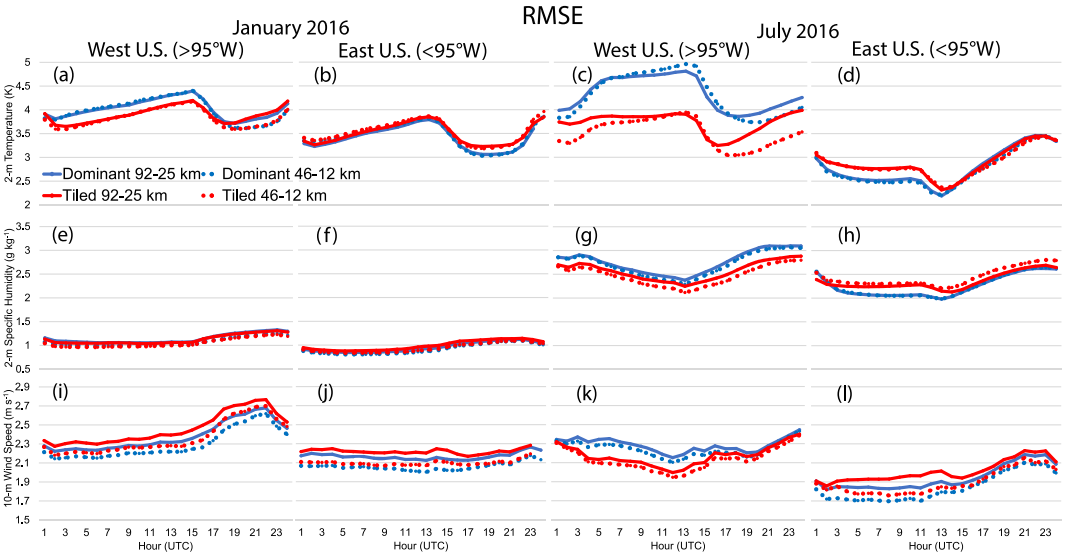

Figure 11. Same as in Figure 10, but for RMSE.

and leads to predominantly drier (ΔQSFC < 0) and warmer surface conditions (ΔTSK > 0) (red and blue lines; Figures 8f–8j). A similar drier and warmer pattern is also true when including tiled fractions of evergreens in cells that are dominated by deciduous forest, as evergreens typically have less daytime transpiration (ΔLH < 0) compared to deciduous trees in July (green lines; Figures 8f–8j). In January, the diurnal patterns of G, LH, SH, QSFC, and TSK in January are similar to July but have smaller amplitudes due to smaller net radiation energy for the U.S. winter and consequently smaller magnitudes for the ΔG, ΔLH, and ΔSH partitioning (Figures 8a–8e).

3.2. Model Evaluations of the MPAS-A Dominant and Tiled LCC Approach

The tiled approach results in widespread reductions in MB for T2, Q2, and WSPD10 across the United States for a 92–25 km mesh during January and July 2016 (Figure 9). The largest and most prolific reductions in MB

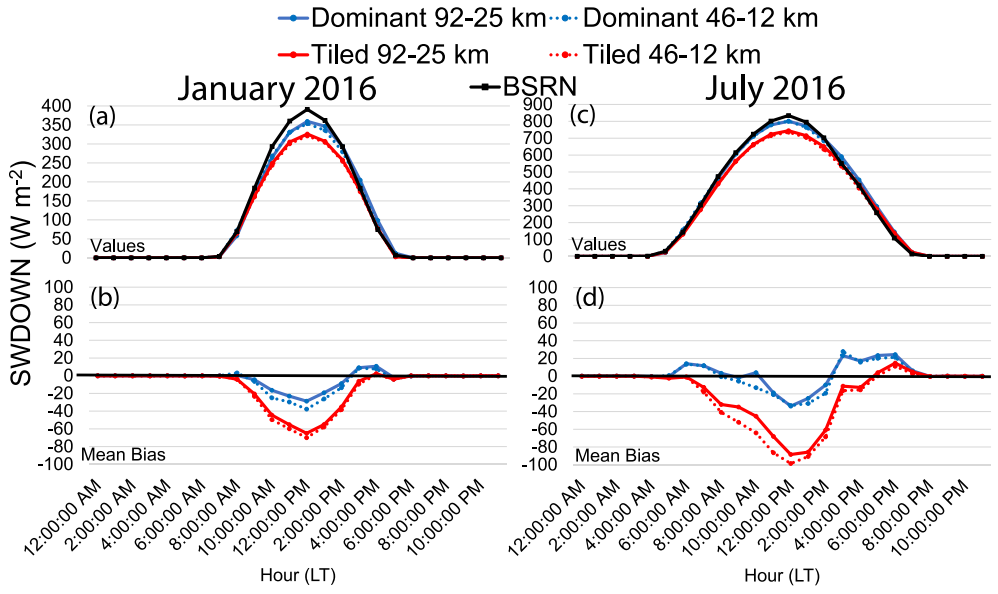

Figure 12. Average diurnal time series of SWDOWN and bias comparisons against BSRN for 10 CONUS sites for both 92–25 and 46–12 km meshes.

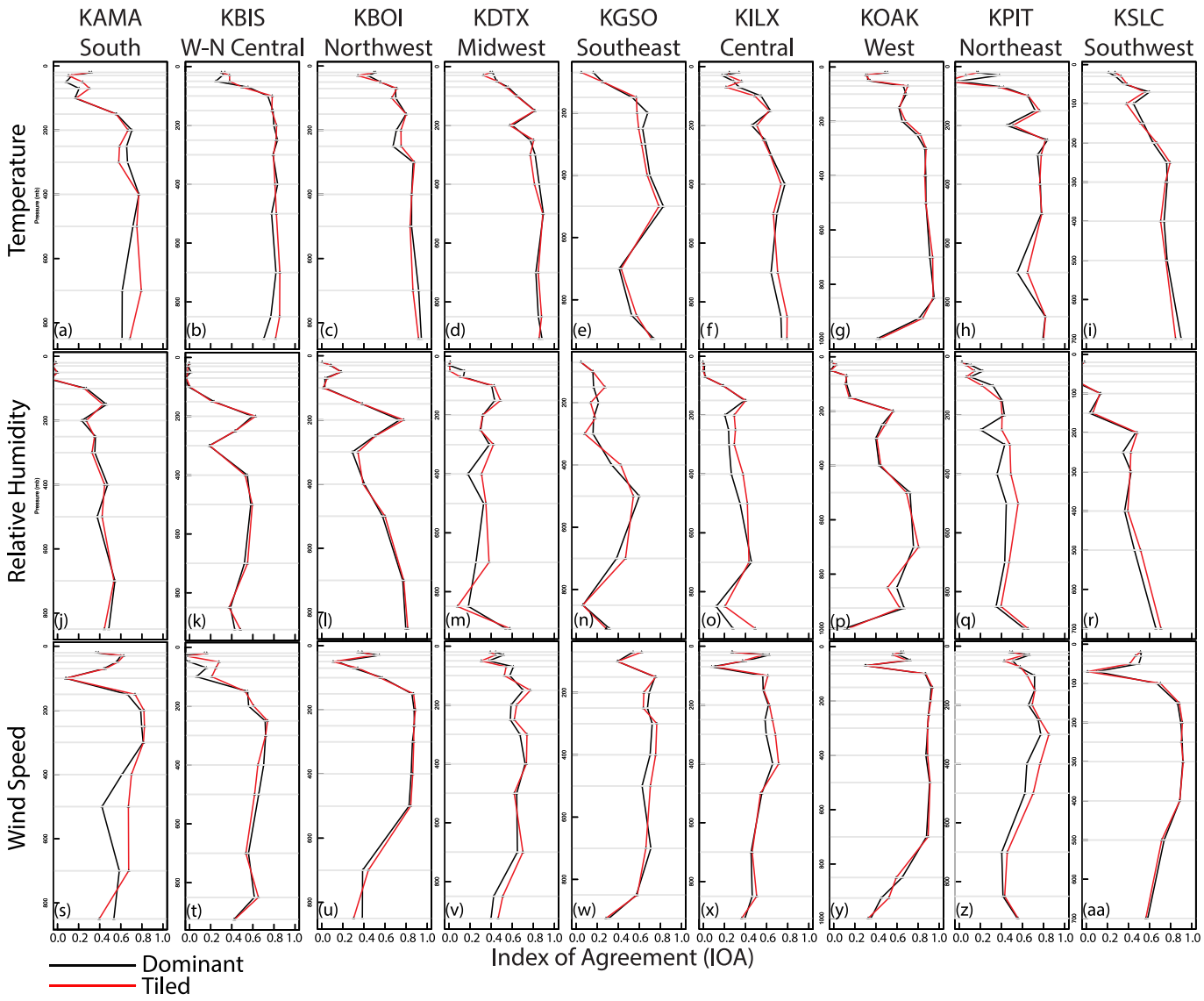

Figure 13. Vertical profiles of IOA compared against select RAOB sites across CONUS for temperature (top), relative humidity (middle), and wind speed (bottom) for the dominant (black) and tiled (red) approach for the 92–25 km mesh.

are found in the western United States in July, where there are large decreases in T2 and increases in Q2 (Figures 9c, 9d, 9g, and 9h). There are some smaller areas of increased MB for T2 and Q2, most notably in the southeast United States for July where increased temperatures exacerbate the simulated warm bias for T2, and in parts of the Central United States where decreases in predicted mixing ratio exacerbate the model dry bias for Q2. While more variable in nature, there are predominantly decreased MB for WSPD10 across the United States. There are also widespread decreases in the RMSE for the tiled approach for T2, Q2, and WSPD10 (supporting information Figure S3). Similar to the global changes (Figure 6), mostly all the major changes in T2, Q2, and WSPD10 are statistically significant in CONUS (p-value $\leq$0.05), with only very localized areas of insignificant changes (i.e., $p > 0.05$).

The results from the 92–25 and 46–12 km meshes show a reduction in diurnal MB and RMSE for T2, Q2, and WSPD10 in the western United States during July, and there is preliminary indication of decreasing model sensitivity to the mesh resolution for T2 when using the tiled approach (i.e., MB red lines closer than blue lines) (Figures 10 and 11); however, testing of more resolutions are necessary for a full investigation of grid sensitivity. The impacts of the tiled approach are less for January in the eastern United States, with some

model degradation for similar reasons as discussed previously. The average CONUS and global statistical summaries (i.e., R, MB, RMSE, and IOA) are found in supporting information Tables S1 and S2. Overall, the largest model performance change in CONUS is for T2, where the average MB is reduced by a factor of ~4 due to the tiled approach. There is also lower MB for the WSPD10 in the western United States for July; however, there are increases in MB and RMSE for Q2 and WSPD10 in the eastern United States. This dipole in model performance change apparent across CONUS is consistent with the strong east-west vegetation and moisture gradient and its interaction with the tiled compared to dominant LCC approaches.

The effects of the tiled LCC approach on the partitioning of SH_flx and LH_flx also have implications for the total incoming SWDOWN (Figure 12).

For an average of 10 BSRN sites across CONUS (supporting information Figure S4 contains a map of the U.S. sites), the tiled approach leads to an overall reduction in total SWDOWN during the local peak time, which leads to an overall increase in MB (and RMSE; see supporting information Figure S5) compared to the dominant LCC approach. This effect is more prominent during summer in July due to appreciable forest fractions included in the dominant shrublands/grasslands across the western United States (Figure 3h) and the resulting increase in EF and Q2 here (Figures 6h and 7d). A spatial evaluation of SWDOWN against the global BSRN observation sites also shows increases in MB and RSME in the early to late afternoon hours due to the tiled approach, particularly in July 2016 for BSRN sites in the Northern Hemisphere (supporting information Figures S6 and S7).

Incorporating more detailed and realistic LCC in MPAS-A leads to widespread model performance improvements (decreased MB and RMSE) for T2 and Q2, particularly in the western United States, but a degradation (increased MB and RMSE) in the evaluation of SWDOWN possibly driven by competing cloud-radiative feedback effects, both in the United States and globally. This result may be indicative of a relatively "tuned" model performance toward more accurate predictions of near-surface temperature and moisture in MPAS-A (and other NWP models), at the expense of degrading performance (and more unknown) for cloud-radiative feedback processes that affect the surface radiative balance (Ma et al., 2014).

The impacts of the tiled approach extend above the surface as well, and there are increases in the IOA for the temperature, relative humidity, and wind speed profiles compared to RAOB sites across CONUS (Figure 13). The tiled approach shows increases in IOA for temperature up to about 500–600 hPa model heights for all the RAOB sites shown except in the northwest (Boise, Idaho; KBOI) and southwest United States (Salt Lake City, UT; KSLC). The relative humidity also shows increased IOA across an increased depth of the atmosphere (up to 200 hPa) for the central (Lincoln, IL; KILX) and northeast United States (Pittsburgh, PA; KPIT) compared to the dominant approach. There are slight decreases in IOA for the tiled approach in the lower atmosphere (>800 hPa) in the upper midwest (Detroit, MI; KDTX) and western United States (Oakland, CA; KOAK), but overall, there are larger increases in IOA compared to the decreases across the RAOB sites (i.e., generally improved model column performance). There are also larger increases in IOA for wind speed compared to the decreases for the tiled approach, where in some cases these increases are across a significant depth of the model column, for example, in the south (Amarillo, TX; KAMA) and northeast United States (KPIT).

4. Summary and Implications

In this work a tiled approach to LCC in the Noah LSM, following Li et al. (2013), is implemented in the MPAS-A, version 6.0, and was tested for January and July 2016 on both the 92–25 and 46–12 km refining meshes (focused on the CONUS). Implementation of the tiled LCC in MPAS shows significant impacts on global soil conditions, surface fluxes, and near-surface atmospheric properties compared to the largely simplified dominant LCC approach. Specifically, the tiled LCC leads to both moderate warming and cooling in the Northern and Southern Hemispheres in January, respectively, with more dramatic, globally widespread cooling in July. For CONUS, there is a strong dichotomy of cooler and moister conditions in the west and warmer and drier conditions in the east due to the tiled LCC. Such temperature and moisture changes are a result of shifts in tiled evergreen and deciduous forests, grasslands/shrublands, and urban LCC in the eastern and western United States compared to the dominant approach, which alter the overall cloud-radiative balance, available energy, and diurnal partitioning between the ground, sensible, and latent heat fluxes.

These changes in turn effect the development of near-surface wind flow, boundary layer heights, cloud formation processes, and resulting cloud-radiative feedbacks.

The tiled LCC has a strong impact on model performance, where there are significant reductions in both MB and RMSE in CONUS for 2-m temperature, 2-m specific humidity, and 10-m wind speed; however, there are increases in model bias and error for incoming solar radiation. There is a preliminary indication that the tiled LCC also reduces the sensitivity of predicted 2-m temperature to the finer 46–12 km mesh resolution in the eastern United States; however, more studies of the mesh sensitivity are necessary. Depending on the specific variable (temperature, relative humidity, or wind speed) and U.S. region, there is also a moderate indication that the tiled LCC impact may extend upward the atmospheric column, while demonstrating improved agreement compared to many radiosonde locations.

An important implication of this work is the effect of the tiled LCC on the evaporative fraction, cloud-radiative feedbacks, and the overall reduction in global temperatures in July (Northern Hemisphere summer). As demonstrated by the improved model performance for 2-m temperature in CONUS, use of a tiled LCC could mitigate the systematic, global summertime warm biases that are apparent in many climate and NWP models, particularly those that apply a dominant LCC approach. The improved near-surface meteorology, but degraded performance in incoming solar radiation due to the more detailed tiled LCC, further demonstrates that NWP models such as MPAS-A have experienced prolonged deficiencies in the LCC representation and processes, while being preferentially "tuned" to improve the above ground meteorological predictions despite unresolved cloud feedbacks. The need for more iterative model developments with respect to LCC methodologies in LSMs and the impacts on soil/surface, meteorological, and cloud feedbacks in NWP models cannot be overstated. While further testing is needed (e.g., a full calendar year and detailed cloud-radiative analysis/evaluation), it is further recommended that computationally efficient subgrid LCC schemes be continually developed and integrated in the LSMs coupled to global weather forecast models.

Data Availability Statement

A pre-release version 1.0.0 of the modified MPAS-A version 6.1 source code, which includes the tiled Noah LCC option, is available online (at https://doi.org/10.5281/zenodo.3734982). The raw and processed MPAS simulation data are very large (total size >10 TB) and are freely available in two different ways: (1) on the local U.S. EPA repositories that can be directly transferred via SFTP or SCP in pieces, or manually copied in their entirety and provided via external hard drives, and (2) on a publicly available repository/transfer in pieces or via another high-speed file transfer service such as Globus (https://www.globus.org/data-transfer).

Disclaimer

Although this work has been reviewed and approved for publication by the U.S. EPA, it does not necessarily reflect the views and policies of the agency.

Acknowledgments
This research was performed while Patrick Campbell held a National Research Council Research Associateship Award at the U.S. Environmental Protection Agency (EPA). We thank Kiran Alapaty and Russell Bullock Jr. (U.S. EPA) and Fantine Ngan (NOAA/ARL) for providing valuable comments on a draft of this manuscript. We further acknowledge the MADIS-METAR, WRMC-BSRN, and ESRL-Observational networks for their data records.

References

Ament, F., & Simmer, C. (2006). Improved representation of land-surface heterogeneity in a non-hydrostatic numerical weather prediction model. *Boundary-Layer Meteorology*, *121*(1), 153–174. https://doi.org/10.1007/s10546-006-9066-4

Avissar, R. (1991). A statistical-dynamic approach to parameterize subgrid scale land-surface heterogeneity in climate models. *Surveys in Geophysics*, *12*(1–3), 155–178. https://doi.org/10.1007/Bf01903417

Avissar, R., & Pielke, R. A. (1989). A parameterization of heterogeneous land surfaces for atmospheric numerical-models and its impact on regional meteorology. *Monthly Weather Review*, *117*(10), 2113–2136. https://doi.org/10.1175/1520-0493(1989)117<2113:APOHLS>2.0.CO;2

Campbell, P. C., Bash, J. O., & Spero, T. L. (2019). Updates to the Noah land surface model in WRF-CMAQ to improve simulated meteorology, air quality, and deposition. *Journal of Advances in Modeling Earth Systems*, *11*(1), 231–256. https://doi.org/10.1002/2018MS001422

Chen, F., & Dudhia, J. (2001). Coupling an advanced land surface-hydrology model with the Penn State-NCAR MM5 modeling system. Part I: Model implementation and sensitivity. *Monthly Weather Review*, *129*, 569–585. https://doi.org/10.1175/1520-0493(2001)129<0569:CAALSH>2.0.CO;2

Chen, F., Janjic, Z., & Mitchell, K. E. (1997). Impact of atmospheric surface-layer parameterizations in the new land-surface scheme of the NCEP mesoscale Eta model. *Bound. Layer Meteorol.*, *85*(3), 391–421. https://doi.org/10.1023/A:1000531001463

Chen, F., Manning, K. W., LeMone, M. A., Trier, S. B., Alfieri, J. G., Roberts, R., et al. (2007). Description and evaluation of the characteristics of the NCAR high-resolution land data assimilation system. *Journal of Applied Meteorology and Climatology*, *46*(6), 694–713. https://doi.org/10.1175/JAM2463.1

Chen, F., Mitchell, K., Schaake, J., Xue, Y., Pan, H. L., Koren, V., et al. (1996). Modeling of land-surface evaporation by four schemes and comparison with FIFE observations. *Journal of Geophysical Research*, *101*(D3), 7251–7268. https://doi.org/10.1029/95JD02165

Driemel, A., Augustine, J., Behrens, K., Colle, S., Cox, C., Cuevas-Agulló, E., et al. (2018). Baseline Surface Radiation Network (BSRN): Structure and data description (1992–2017). *Earth System Science Data*, *10*(3), 1491–1501. https://doi.org/10.5194/essd-10-1491-2018

Ek, M. B., Mitchell, K. E., Lin, Y., Rogers, E., Grunmann, P., Koren, V., et al. (2003). Implementation of Noah land surface model advances in the National Centers for Environmental Prediction operational mesoscale Eta model. *Journal of Geophysical Research*, *108*(D22), D22. https://doi.org/10.1029/2002JD003296

Emery, C., Liu, Z., Russell, A. G., Odman, M. T., Yarwood, G., & Kumar, N. (2017). Recommendations on statistics and benchmarks to assess photochemical model performance. *Journal of the Air & Waste Management Association*, *67*(5), 582–598. https://doi.org/10.1080/10962247.2016.1265027

Entekhabi, D., & Eagleson, P. S. (1989). Land surface hydrology parameterization for atmospheric general circulation models including subgrid scale spatial variability. *Journal of Climate*, *2*(8), 816–831. https://doi.org/10.1175/1520-0442(1989)002<0816:Lshpfa>2.0.Co;2

Famiglietti, J. S., & Wood, E. F. (1991). Evapotranspiration and runoff from large land areas: Land surface hydrology for atmospheric general circulation models. *Surveys in Geophysics*, *12*(1–3), 179–204. https://doi.org/10.1007/Bf01903418

Giorgi, F., & Avissar, R. (1997). Representation of heterogeneity effects in earth system modeling: Experience from land surface modeling. *Reviews of Geophysics*, *35*(4), 413–437. https://doi.org/10.1029/97RG01754

Gollvik, S., & Samuelsson, S. (2011). *A tiled land-surface scheme for HIRLAM*. Norrkoping, Sweden: Swedish Meteorological and Hydrological Institute.

Hibbard, K. A., Hoffman, F. M., Huntzinger, D., & West, T. O. (2017). Changes in land cover and terrestrial biogeochemistry. In D. J. Wuebbles, D. W. Fahey, K. A. Hibbard, D. J. Dokken, B. C. Stewart, & T. K. Maycock (Eds.), *Climate science special report: Fourth National Climate Assessment, volume I* (pp. 277–302). Washington, DC, USA: U.S. Global Change Research Program. https://doi.org/10.7930/J0416V6X

Koster, R. D., & Suarez, M. J. (1992). A comparative analysis of two land surface heterogeneity representations. *Journal of Climate*, *5*(12), 1379–1390. https://doi.org/10.1175/1520-0442(1992)005<1379:Acaotl>2.0.Co;2

Li, D., Bou-Zeid, E., Barlage, M., Chen, F., & Smith, J. A. (2013). Development and evaluation of a mosaic approach in the WRF-Noah framework. *Journal of Geophysical Research: Atmospheres*, *118*(21), 11,918–11,935. https://doi.org/10.1002/2013JD020657

Li, H., Wolter, M., Wang, X., & Sodoudi, S. (2017). Impact of land cover data on the simulation of urban heat island for Berlin using WRF coupled with bulk approach of Noah-LSM. *Theoretical and Applied Climatology*, *134*(1–2), 67–81. https://doi.org/10.1007/s00704-017-2253-z

Li, R., & Arora, V. K. (2012). Effect of mosaic representation of vegetation in land surface schemes on simulated energy and carbon balances. *Biogeosciences*, *9*(1), 593–605. https://doi.org/10.5194/bg-9-593-2012

Ma, H., Xie, S., Klein, S. A., Williams, K. D., Boyle, J. S., Bony, S., et al. (2014). On the correspondence between mean forecast errors and climate errors in CMIP5 models. *Journal of Climate*, *27*(4), 1781–1798. https://doi.org/10.1175/JCLI-D-13-00474.1

Mallard, M. S., & Spero, T. L. (2018). Effects of mosaic land use on dynamically downscaled WRF simulations of the contiguous United States. *Journal of Geophysical Research: Atmospheres*, *124*(16), 9117–9140. https://doi.org/10.1029/2018JD029755

Manrique-Suñén, A., Nordbo, A., Balsamo, G., Beljaars, A., & Mammarella, I. (2013). Representing land surface heterogeneity: Offline analysis of the tiling method. *Journal of Hydrometeorology*, *14*(3), 850–867. https://doi.org/10.1175/JHM-D-12-0108.1

Masson, V., le Moigne, P., Martin, E., Faroux, S., Alias, A., Alkama, R., et al. (2013). The SURFEXv7.2 land and ocean surface platform for coupled or offline simulation of earth surface variables and fluxes. *Geoscientific Model Development*, *6*(4), 929–960. https://doi.org/10.5194/gmd-6-929-2013

Melton, J. R., & Arora, V. K. (2014). Subgrid scale representation of vegetation in global land surface schemes: Implications for estimation of the terrestrial carbon sink. *Biogeosciences*, *11*(4), 1021–1036. https://doi.org/10.5194/bg-11-1021-2014

Mitchell, K. E., Lohmann, D., Houser, P. R., Wood, E. F., Schaake, J. C., Robock, A., et al. (2004). The multi-institution North American Land Data Assimilation System (NLDAS): Utilizing multiple GCIP products and partners in a continental distributed hydrological modeling system. *Journal of Geophysical Research: Atmospheres*, *109*, D07S90. https://doi.org/10.1029/2003JD003823

Morcrette, C. J., Van Weverberg, K., Ma, H.-Y., Ahlgrimm, M., Bazile, E., Berg, L. K., et al. (2018). Introduction to CAUSES: Description of weather and climate models and their near-surface temperature errors in 5 day hindcasts near the Southern Great Plains. *Journal of Geophysical Research: Atmospheres*, *123*(5), 2655–2683. https://doi.org/10.1002/2017JD027199

Newman, A. J., Clark, M. P., Winstral, A., Marks, D., & Seyfried, M. (2014). The use of similarity concepts to represent subgrid variability in land surface models: Case study in a snowmelt-dominated watershed. *Journal of Hydrometeorology*, *15*(5), 1717–1738. https://doi.org/10.1175/JHM-D-13-038.1

Niu, G.-Y., Yang, Z.-L., Mitchell, K. E., Chen, F., Ek, M. B., Barlage, M., et al. (2011). The community Noah land surface model with multiparameterization options (Noah-MP): 1. Model description and evaluation with local-scale measurements. *Journal of Geophysical Research: Atmospheres*, *116*, D12109. https://doi.org/10.1029/2010JD015139

Pan, H.-L., & Mahrt, L. (1987). Interaction between soil hydrology and boundary layer development. *Boundary-Layer Meteorology*, *38*(1-2), 185–202. https://doi.org/10.1007/BF00121563

Powers, J. G., Klemp, J. B., Skamarock, W. C., Davis, C. A., Dudhia, J., Gill, D. O., et al. (2017). The Weather Research and Forecasting Model: Overview, system efforts, and future directions. *Bulletin of the American Meteorological Society*, *98*(8), 1717–1737. https://doi.org/10.1175/BAMS-D-15-00308.1

Samuelsson, S., Gollvik, S., & Ullerstig, A. (2006). The land surface scheme of the Rossby Centre Regional Atmospheric Climate Model (RCA3). *Meteorology* (Vol. *122*, pp. 1-25). Norrkoping, Sweden: SMHI.

Skamarock, W. C., & Klemp, J. B. (2008). A time-split nonhydrostatic atmospheric model for weather research and forecasting applications. *Journal of Computational Physics*, *227*(7), 3465–3485. https://doi.org/10.1016/j.jcp.2007.01.037

Skamarock, W. C., Klemp, J. B., Duda, M. G., Fowler, L. D., Park, S., & Ringler, T. D. (2012). A multiscale nonhydrostatic atmospheric model using centroidal Voronoi tesselations and C-grid staggering. *Monthly Weather Review*, *140*(9), 3090–3105. https://doi.org/10.1175/MWR-D-11-00215.1

Steiner, A. (2018). Diagnosing the warm bias in the Central United States. *Eos*, *99*, https://doi.org/10.1029/2018eo095669

Verseghy, D. L., McFarlane, N. A., & Lazare, M. (1993). CLASS—A Canadian land surface scheme for GCMs. 2. Vegetation model and coupled runs. *International Journal of Climatology*, *13*(4), 347–370. https://doi.org/10.1002/joc.3370130402

Yin, J., Zhan, X., Zheng, Y., Hain, C., Ek, M., Wen, J., et al. (2015). Improving Noah land surface model performance using near real time surface albedo and green vegetation fraction. *Agricultural and Forest Meteorology*, 171–183. https://doi.org/10.1016/j.agrformet.2015.12.001